# Stress-driven thermohaline loops

Shaoyu Yuan[a)]
*MIT/WHOI Joint Program in Physical Oceanography, Massachusetts Institute of Technology, Cambridge, Massachusetts 02139*

Carl Wunsch
*Department of Earth, Atmospheric and Planetary Sciences, Massachusetts Institute of Technology, Cambridge, Massachusetts 02139*

(Received 2 February 2005; accepted 14 April 2005; published online 27 May 2005)

The two-state Stommel box model, commonly invoked as an ocean circulation analog, is dynamically equivalent to a one-dimensional fluid loop (called "loop-Stommel" models). Although it dominates the energy input to the ocean circulation, the wind stress is usually omitted from the discussion. Here we briefly explore the behavior of loop-Stommel models in the presence of stress, with both thermal and salinity sources. Although the unstable (Rayleigh–Bénard) configuration is considered, most interest lies with buoyancy sources at the same geopotential (type 3 convection). In addition to the nondimensional stress, the multiple solutions depend upon the Rayleigh and Prandtl numbers with the latter primarily determining the stability of the possible steady states. Salinity forcing in a double-diffusive configuration introduces another stable mode.
 [DOI: 10.1063/1.1927887]

## I. INTRODUCTION

The two-box model of Stommel[1] (called S61) has often been used to represent and analyze the ocean circulation and its climate role. This model, with various modifications, displays multiple equilibria and other interesting behaviors. Three-, four-, eight-, and even sixteen-box models[2–4] were subsequently formulated to increase both the horizontal and vertical resolutions, but whether multiple box models more closely represent the ocean is unknown.

A superficially different class of fluid models is that of one-dimensional fluid loops. Such models have applications in solar-heated water systems, nuclear reactors, and geothermal energy systems, and have been widely studied (often called "thermosyphons"). The heated loop system exhibits several interesting features including instabilities and chaos,[5–9] and is easier to analyze than the S61 model.

Kinematically and dynamically, however, the original Stommel model is isomorphic to the one-dimensional flow in a fluid loop, as has been recognized by a number of authors, including, e.g., Welander.[6] In two recent papers,[10,11] the behavior of the fluid loop was exploited to understand the behavior of what is meant to be the physical analog of the S61 model to the full ocean circulation. Temperature and salinity forcing were used, and a stress component was introduced to represent the wind field. Earlier, Stommel and Rooth[12] had briefly described the influence of stress on a purely thermally driven version of the S61 model. The context of some of the recent discussions of wind stress influence on mass and heat transport properties of the ocean arises from the growing realization[13–16] that purely buoyancy-driven circulations in an ocean configuration, where heating and cooling are at the same geopotential, raises serious issues of energetics and thermodynamics. Altogether, this literature concerns the extent to which the ocean can have a significant "thermohaline circulation"[17] in the absence of an energetically dominant wind stress driving? An alternative energy source for the observed circulation lies with tidal forcing.[13] Wunsch[11] discussed the shifts in ocean circulation that could occur given a major change in tidally governed deep-ocean mixing, as might have occurred during the last deglacial period. The wind field, however, appears ultimately to be a much greater source of energy[18,19] and general circulation theories of the ocean are dominated by the effects of wind.[20]

The purpose of this paper is thus to more fully, but briefly, understand the behavior of "loop-Stommel" models (the term we use for the generalized one-dimensional system representing both S61 type models and loop configurations) in the presence of buoyancy forcing (temperature and salinity) and a stress field. We explore the role stress plays in the loop-Stommel system, with a focus on type 1 and type 3 convection (in the terminology of Wunsch and Ferrarri[18]). Some configurations, such as the loop heated in the Rayleigh–Bénard configuration, lead to a Lorenz[21] system; more generally, we will discuss the existence of multiple equilibria and their stability.

## II. A SIMPLE MODEL

The same circular loop as discussed by Wunsch[10,11] (see Fig. 1) is used. $\phi$ is measured along the loop from $\phi=-\pi$ at the lowest point around the loop anticlockwise with $\phi=0$ at the highest point. Assume that the loop is sufficiently thin such that the flow is everywhere the same, and denote it by $w$ to be suggestive of an oceanic overturning velocity. A heat source is applied at $\phi_+$ and a cooling one at $\phi_-$.

The governing equations for temperature $T$ and salinity $S$ are

[a)]Electronic mail: syuan@mit.edu

 

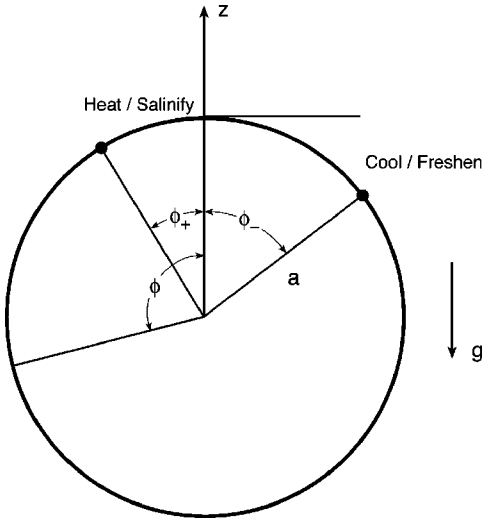


FIG. 1. Model schematic [from the work of Wunsch (Refs. 10 and 11)]. The system consists of a loop with heating and cooling sources at $\phi=\phi_\pm$. The azimuthal angle $\phi$ is measured relative to the loop top and the gravity force is downward. The loop radius is $a$.

$$\frac{\partial T}{\partial t}+\frac{w}{a}\frac{\partial T}{\partial \phi}-\frac{\kappa_T}{a^2}\frac{\partial^2 T}{\partial \phi^2}=2\pi T_0[\delta(\phi-\phi_+)-\delta(\phi-\phi_-)]h(t), \tag{1}$$

$$\frac{\partial S}{\partial t}+\frac{w}{a}\frac{\partial S}{\partial \phi}-\frac{\kappa_S}{a^2}\frac{\partial^2 S}{\partial \phi^2}=2\pi S_0[\delta(\phi-\phi_+)-\delta(\phi-\phi_-)]h(t), \tag{2}$$

where $\kappa_T$ and $\kappa_S$ are the thermal and salinity diffusivities. $\delta(\phi)$ is the Dirac delta function; $T_0$ and $S_0$ are dimensional constants. $h(t)$ is the Heaviside function, making it possible to study the evolution of the system when heat and salt source/sinks turn on at $t=0$.

The momentum equation, in the Boussinesq approximation, is

$$\frac{\partial w}{\partial t}=-\frac{\partial p}{a\rho_0\,\partial\,\phi}+g\frac{\rho}{\rho_0}\sin\phi-\epsilon w+\tau, \tag{3}$$

where $\epsilon$ is a Rayleigh friction coefficient. In this limit, the stress $\tau$ is an externally prescribed body force used to mimic the effects wind stress plays in the ocean.

For maximum simplicity, density is calculated using a linear equation of state

$$\rho(\phi,t)=\rho_0[1-\Delta_T T(\phi,t)+\Delta_S S(\phi,t)].$$

Integrating Eq. (3) around the loop yields

$$\frac{\partial w}{\partial t}=\frac{g}{2\pi}\int_{-\pi}^{\pi}[-\Delta_T T(\phi)+\Delta_S S(\phi)]\sin\phi\,d\phi-\epsilon w+\tau. \tag{4}$$

The system is now nondimensionalized,

$$T=\frac{a^2}{\kappa_T}T_0T',\quad S=\frac{a^2}{\kappa_S}S_0S',\quad w=\frac{\kappa_T}{a}w',\quad t=\frac{a^2}{\kappa_T}t',$$

$$\tau=\frac{\epsilon\kappa_T}{a}\tau',$$

producing

$$\frac{\partial T}{\partial t}+w\frac{\partial T}{\partial \phi}-\frac{\partial^2 T}{\partial \phi^2}=2\pi[\delta(\phi-\phi_+)-\delta(\phi-\phi_-)]h(t), \tag{5}$$

$$\frac{\partial S}{\partial t}+w\frac{\partial S}{\partial \phi}-\lambda\frac{\partial^2 S}{\partial \phi^2}=2\pi[\delta(\phi-\phi_+)-\delta(\phi-\phi_-)]h(t), \tag{6}$$

$$\frac{1}{P_r}\frac{\partial w}{\partial t}=\frac{R_a}{2\pi}\int_{-\pi}^{\pi}\left(-T(\phi)+\frac{D}{\lambda}S(\phi)\right)\sin\phi\,d\phi-w+\tau, \tag{7}$$

$$R_a=\frac{ga^3\Delta_T T_0}{\epsilon\kappa_T^2},\quad P_r=a^2\epsilon/\kappa_T,\quad D=\frac{\Delta_S S_0}{\Delta_T T_0},\quad \lambda=\kappa_S/\kappa_T,$$

where the primes have been dropped from the nondimensional variables. $R_a$ and $P_r$ are the Rayleigh number and Prandtl number for the loop model,[10] and $\lambda$ is the Lewis number, the ratio of the salinity diffusivity $\kappa_S$ to the thermal diffusivity $\kappa_T$. The nondimensionalization differs from that used previously, but proves slightly more convenient for present purposes. Equations (5)–(7) form the basic nondimensional equation set that will be used in the following discussion.

## III. THERMAL FORCING WITH STRESS

Fluid loops (rectangular or circular) driven by purely thermal flux have been investigated in great detail. To study most simply the interaction between stress and thermal forcing, salinity is temporarily suppressed. Wunsch[10] discussed steady solutions of this type, but the transient behavior and the stability properties of the steady solutions need further investigation. Since $T$ is necessarily periodic in $\phi$ along the loop,[7,10] the solution can be written as

$$T(\phi,t)=\sum_{n=-\infty}^{\infty}\alpha_n(t)e^{in\phi}. \tag{8}$$

Substituting into Eq. (5), one readily finds that for $\alpha_{\pm1}$

$$\frac{d\alpha_1(t)}{dt}=(-iw-1)\alpha_1+e^{-i\phi_+}-e^{-i\phi_-}, \tag{9}$$

$$\frac{d\alpha_{-1}(t)}{dt}=(iw-1)\alpha_{-1}+e^{i\phi_+}-e^{i\phi_-}, \tag{10}$$

and the integrated form of (7) becomes

$$\frac{2\pi}{P_r}\frac{dw}{dt} = -R_a\int_{-\pi}^{\pi}[\alpha_1(t)e^{i\phi} + \alpha_{-1}(t)e^{-i\phi}]\sin\phi\, d\phi - 2\pi w + 2\pi\tau. \quad (11)$$

If $\alpha_1$ is written as $\alpha_1 = a_1 + ib_1$, following Malkus,[7] we obtain the resulting equations describing the time-dependent system:

$$\frac{1}{P_r}\frac{dw}{dt} = R_a b_1 - w + \tau, \quad (12)$$

$$\frac{da_1}{dt} = -a_1 + b_1 w + \cos\phi_+ - \cos\phi_-, \quad (13)$$

$$\frac{db_1}{dt} = -b_1 - a_1 w - \sin\phi_+ + \sin\phi_-. \quad (14)$$

Setting the time derivative terms in Eqs. (12)–(14) to zero yields the steady solutions for the system, as the roots $w$ of the cubic equation

$$-wR_a\frac{\cos\phi_+ - \cos\phi_-}{1+w^2} - R_a\frac{\sin\phi_+ - \sin\phi_-}{1+w^2} = w - \tau. \quad (15)$$

### A. A chaotic system

Let $\alpha = P_r$, $r = R_a(\cos\phi_- - \cos\phi_+)$. $r$ is a measure of the thermal forcing strength. The linear transformation, $x = w$, $y = b_1 R_a$, $z = a_1 R_a + r$, leads to

$$\frac{dx}{dt} = \alpha(y - x + \tau),$$

$$\frac{dy}{dt} = rx - y - xz + (\sin\phi_- - \sin\phi_+)R_a,$$

$$\frac{dz}{dt} = xy - z, \quad (16)$$

and the steady solutions for $x$ are given by

$$x^3 - \tau x^2 + (1-r)x + R_a(\sin\phi_+ - \sin\phi_-) - \tau = 0. \quad (17)$$

#### 1. Free Lorenz system

If the stress is removed, $\tau = 0$, and $\phi_+$ and $\phi_-$ satisfy $\phi_+ = \pi - \phi_-$, $0 \leqslant \phi_- < \pi/2$, that is, heating below cooling—the Rayleigh–Bénard configuration, the equations can be reduced to the Lorenz[21] equations

$$\frac{dx}{dt} = \alpha(y - x),$$

$$\frac{dy}{dt} = rx - y - xz,$$

$$\frac{dz}{dt} = xy - bz, \quad (18)$$

with $b = 1$. With appropriate parameters, chaotic behavior is expected. Putting the heat source at $\phi_+ = \pi$ and the cooling source at $\phi_- = 0$ recovers the case discussed by Tritton.[22] We will not dwell on this much-studied system.

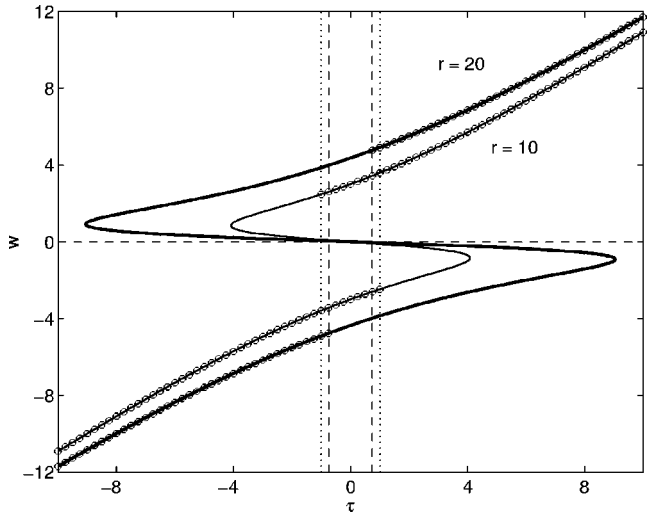


FIG. 2. Roots of Eq. (19) for $w(\tau)$ for varying $r$ with $P_r = 10$. Lines marked by circles suggest the solutions are stable and thereafter. When $r = 10$ (thin line), two of the three solutions are stable between the two vertical dotted lines; when $r = 20$ (thick line), none of the three solutions is stable between the two vertical dashed lines.

#### 2. Lorenz system with stress

As shown in Eq. (16), the forcing terms in the governing equations can be attributed either to the stress term or to the asymmetry of the heat forcing. For the case $\phi_+ = \pi$ and $\phi_- = 0$ (type 1 convection) with stress, Eq. (17) reduces to

$$x^3 - \tau x^2 + (1-r)x - \tau = 0. \quad (19)$$

When $r = 0$, there is no thermal forcing, and the basic balance is between stress and friction, so that the steady solution is necessarily $w = \tau$. The steady solutions and their stability properties corresponding to $r = 10$ and $r = 20$ are displayed in Fig. 2. Lines marked by circles indicate the solutions are stable to small perturbations (stability properties are determined by a regular stability analysis, see Appendix A). Multiple steady states (Fig. 2) are found between the two vertical dotted lines; when $r = 20$, there are no stable steady solutions between the two dashed lines. The nonexistence of steady stable states enriches the behavior of the system.

For greater clarity, the bifurcation diagram corresponding to $\tau = 0$ and $\tau = 1$ is shown in Fig. 3. If $\tau = 0$ (thin line), there is a supercritical pitchfork bifurcation[23] at $r = 1$. But when $r > 17.5$, all three solutions become unstable. When stress is applied, the pitchfork disconnects into two pieces. With thermal forcing increasing from zero, the lower branch is not accessible without large disturbances. Similarly, when $r > 21.3$, there are again no stable steady solutions. Further investigation shows that for moderate $\tau$, a parameter range of multiple equilibria and chaos can be found. As an example, the time evolution of $x$ and $y$ for a specific parameter set $\sigma = 10$, $r = 20$, and $\tau = 1$ is shown in Fig. 4, which is evidently chaotic.

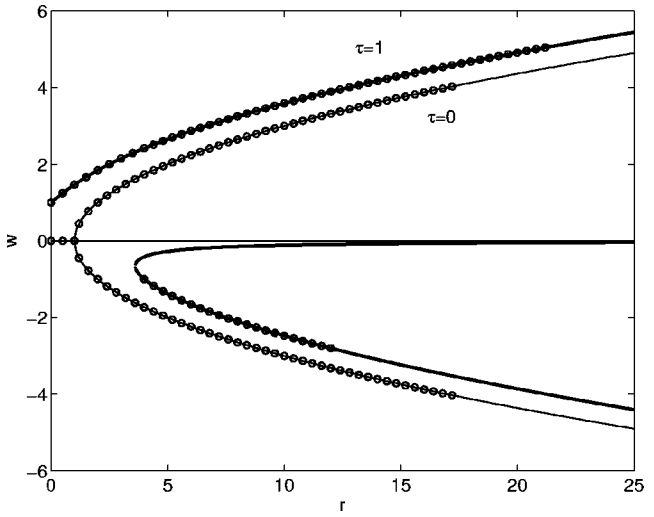


FIG. 3. Bifurcation diagram of $w(r)$ with $P_r=10$. When $\tau=0$, a supercritical pitchfork bifurcation at $r=1$ is found (thin lines), and if $r>17.5$, all the solutions are unstable; when $\tau=1$, the pitchfork disconnects into two pieces (thick lines), and if $r>21.3$, all the solutions are unstable.

Without stress, chaotic behavior can also exist with asymmetric heating. For simplicity, setting $\phi_+=\pi$ leads to

$$x^3+(1-r)x-R_a\sin\phi_-=0. \tag{20}$$

By analyzing this equation and the corresponding solution properties, we can find chaotic behavior and multiple equilibria in some parameter ranges. Further investigation shows that with both stress and asymmetric heat forcing, the resulting equations are similar to those analyzed by Palmer,[24] and the behavior he discussed is expected here in the appropriate parameter ranges.

Type 1 convection is of interest in its own right. Its applicability to the ocean would be through the effects of geothermal heating, but the oceanic response is of second order.[25]

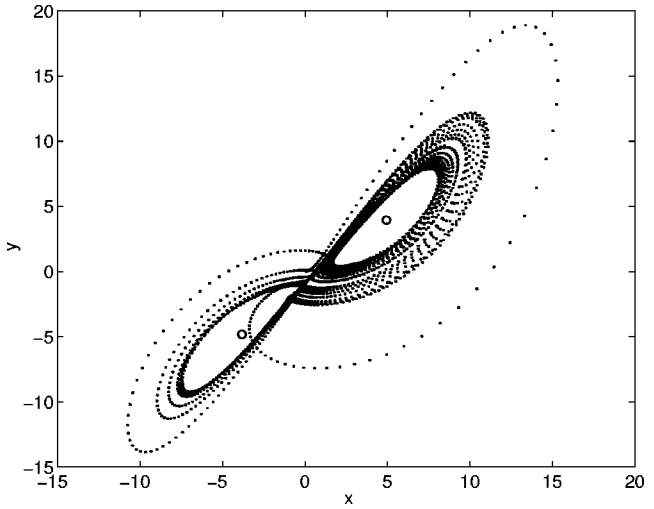


FIG. 4. The evolution of $x$ and $y$ in phase space with zero initial conditions. Here $P_r=10$, $r=20$, and $\tau=1$.

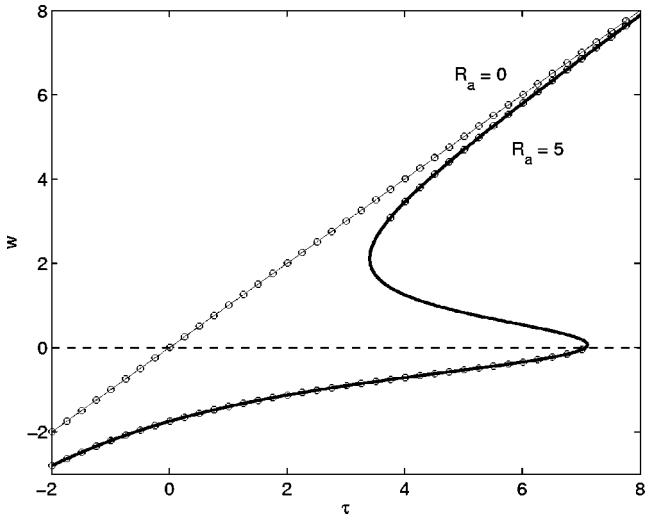


FIG. 5. Roots of Eq. (21) for $w(\tau)$ for varying $R_a$ with $P_r=10$. Thin line indicates $R_a=0$; thick line suggests $R_a=5$.

### B. Oceanic analog

A more direct ocean analog puts the heating and the cooling points at the same level, $\phi_+=-\phi_-=\pi/4$ (type 3 convection), with stress. The effects of the stress on the system and the model sensitivity to other parameters are of interest. In this case, $r=0$, and Eq. (17) reduces

$$w^3-\tau w^2+w-\tau+\sqrt{2}R_a=0. \tag{21}$$

The two parameters $\tau$ and $R_a$ determine the steady flow rates, whose stability properties are affected by the Prandtl number $P_r$. Figure 5 shows $w(\tau)$ corresponding to different Rayleigh numbers with $P_r=10$. When $R_a=0$, the circulation is driven only by stress. When $R_a=5$, the thermal contribution becomes significant. With $\tau<0$, both thermal forcing and stress act together to drive the flow clockwise, making the upper level fluid flow from warm to cold. Although the curve of $w(\tau)$ shifts quantitatively from the no-stress case (see Wunsch[10] for a more specific discussion), no new behavior appears. However, in natural convective systems, such as estuaries and ocean gyres, the applied wind stress tends at least in part to oppose the buoyancy forces, which suggests $\tau>0$. Figure 5 displays with $R_a=5$ (thick line) that multiple states are possible in the range $3.4<\tau<7.1$. $\tau$ has to be strong enough to compete with the thermally forced flow, but not so strong that the thermally forced motion will be totally suppressed.

To see the behavior more clearly, stability diagrams in parameter space are shown in Fig. 6: in the dotted region, two of the three solutions are stable, indicating multiple equilibria; in the dark triangular region, one of the three solutions is stable; elsewhere, only one, stable, solution exists. The dashed line corresponds to the example given in Fig. 5.

#### *1. Dependence of final state on stress $\tau$*

As shown in Fig. 5 with $R_a=5$ (thick line), if the stress is gradually increased from zero, the clockwise flow rate decreases gradually until a critical $\tau=\sqrt{2}R_a$ is reached, where the circulation stalls, as discussed by Stommel and Rooth.[12]

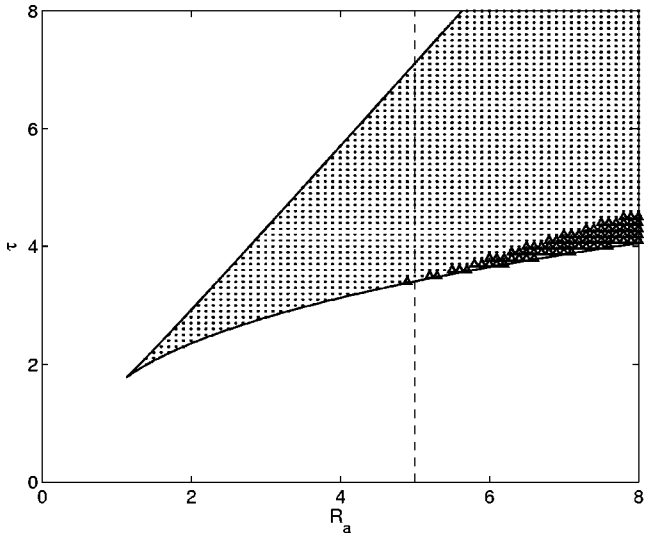


FIG. 6. Stability diagrams in parameter space $R_a$ and $\tau$ with $P_r=10$. In the dotted region, two of the three solutions are stable; in the dark triangular region, one of the three solutions are stable; in other regions, only one, stable, solution exists.

If the stress is increased further, the circulation will jump from the lower to the higher branch and its direction is reversed. If the stress is decreased from a high value, a similar jump occurs.

As an example, let the applied stress be $\tau=5$ initially, with zero initial conditions and $P_r=10$, $R_a=5$. When the system becomes steady, the stress is decreased to $\tau=4$ and then to $\tau=3$. The flow transitions from a stress-driven mode to a thermally driven one (Fig. 7), which implies that small changes in stress can lead to radically different behaviors. However, if the applied stress is $\tau=3$ initially, and increased to $\tau=4$ and then $\tau=5$, the steady states change little (the system remains in a stress-driven mode), showing the dependence of the final states on the initial conditions.

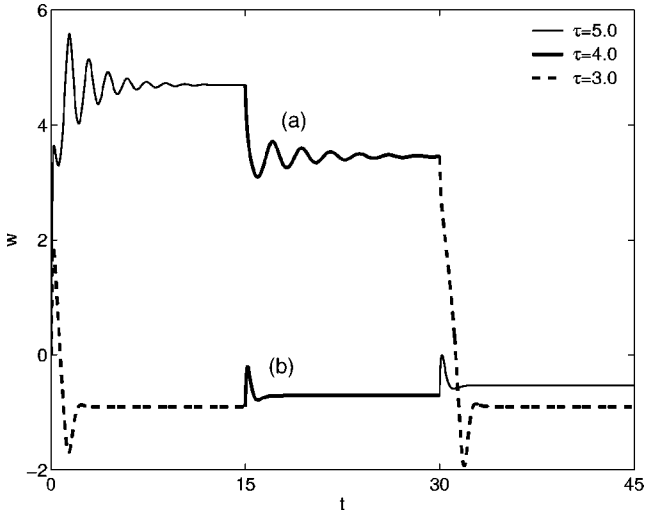


FIG. 7. Time evolution of $w(t)$ with zero initial conditions. In the first case (a), stress is decreased from $\tau=5$ to 4 and 3; in the second case (b), stress is increased from $\tau=3$ to 4 and 5. Within each step, a steady state is reached. $R_a=5$, $P_r=10$ for both cases.

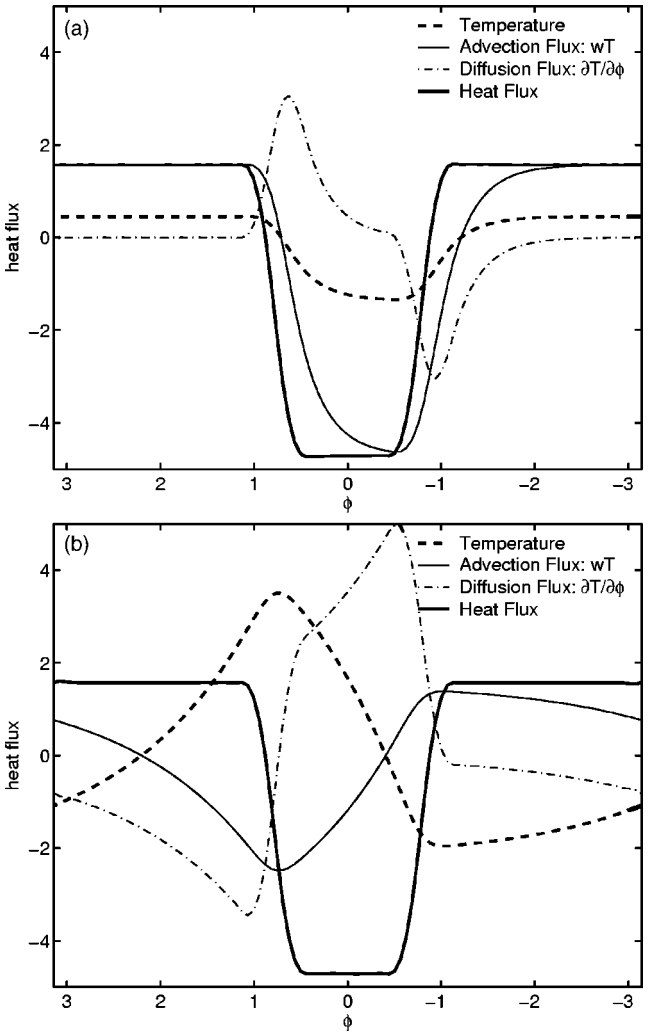


FIG. 8. Temperature distribution and heat flux in the steady states corresponding to different modes. (a) Stress-driven mode; (b) thermally driven mode. Here, $R_a=5$, $P_r=10$, and $\tau=4$.

Figure 5 shows that when the circulation is in a stress-driven mode, $w$ is only slightly smaller than that with $R_a=0$, implying that the buoyancy contribution is very small. The temperature distribution in the loops corresponding to the two different modes is shown in Fig. 8. If, as in the work of Wunsch,[10] the present loop is mapped onto a pseudo-oceanographic form with the two regions, $\pi/4 \leqslant \phi \leqslant \pi$ and $-\pi \leqslant \phi \leqslant -\pi/4$, as though they were a tropical and polar oceanic box, then it is evident that in the stress-driven mode both boxes are weakly stratified, consistent with what Fig. 5 implies (buoyancy effects are weak). In contrast, in the thermally driven mode, there is a strong stratification in the tropical box, but a weak stratification in the polar box, so the resulting buoyancy effect becomes the dominant driving force in the system.

It is of interest to investigate the heat transports $F(\phi)=wT-\partial T/\partial\phi$ corresponding to the different modes. In this model, heat flux is externally applied, with heat transported from $\phi=\pi/4$ to $\phi=-\pi/4$. Although the model exhibits multiple states in the sense of the circulation, the heat transports, however, must remain unchanged in different modes in a

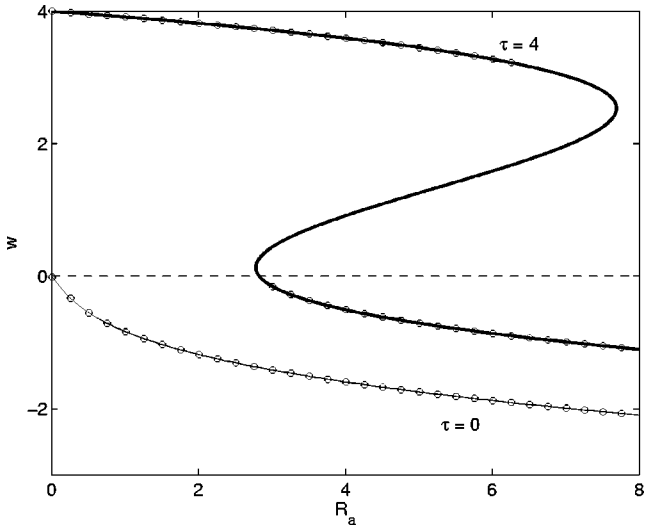


FIG. 9. Roots of Eq. (21) for $w(R_a)$ for varying $\tau$ with $P_r=10$ corresponding to $\tau=0$ (thin line) and $\tau=4$ (thick line).

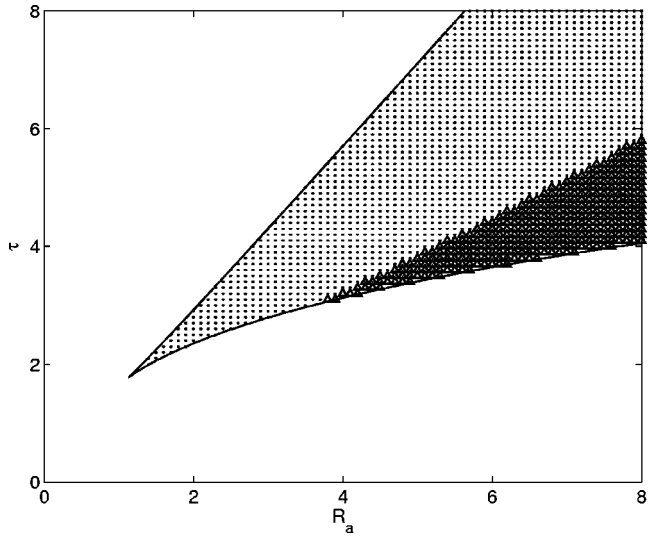


FIG. 10. Stability diagrams in parameter space $R_a$ and $\tau$ with infinitely large Prandtl number. In the dotted region, two of the three solutions are stable; in the dark triangular region, one of the three solutions is stable; in other regions, only one, stable, solution exists.

steady state (Fig. 8). Further exploration (Appendix B) shows that $F(\phi)=\pi/2$ in the upper branch, and $F(\phi)=-3\pi/2$ in the lower branch, whose ratio does not shift no matter how the controlling parameters change. In a steady state, advection and diffusion always compensate to produce the correct total.

If the loop model is considered an analog of multistate ocean circulation (without salinity in this case), it implies that a slight change of the wind stress can lead to totally different modes. Once the system is forced across a threshold, it tends to stay in the new mode, even when the wind stress is restored to its original value.

### 2. Dependence of final state on Rayleigh number $R_a$

Wunsch[10] gave a detailed discussion of the thermally driven circulation. Here the case with $\tau=0$ (Fig. 9) is shown only for completeness. When $R_a=0$, there is no circulation. As $R_a$ grows, the circulation rate also increases.

When positive stress is applied (Fig. 9, $\tau=4$), multiple steady states are found as expected in the parameter range $2.8<R_a<7.7$. Numerical integration shows that a slight change in $R_a$ can also lead to a transition from a thermally driven mode to a stress-driven mode and vice versa.

### 3. Dependence of final state on Prandtl number $P_r$

As already noted, $\tau$ and $R_a$ determine the steady solutions of the system, and $P_r$ affects the stability properties of these solutions. Figure 10 is similar to Fig. 6 but now with infinitely large $P_r$. One infers that with smaller inertia (larger $P_r$), the circulation tends to become more unstable. As an example, consider the transient behavior of the system ($R_a=6, \tau=4, P_r=20$) with initial conditions $w=3.278$, $a_1=-0.395$, $b_1=-0.12$ shown in Fig. 11. The initial conditions are one of the stable steady states corresponding to $P_r=10$. When $P_r=20$, this mode is no longer stable, and the circulation undergoes a transition to become a thermally driven mode.

An important inference from the analysis above is that the initial conditions will determine the final states of the system if all the controlling parameters are fixed. Figure 12 shows the time evolution of $a_1$ and $b_1$ with different initial conditions in phase space. The parameters are $\tau=4$, $R_a=3$, and $P_r=+\infty$, which implies that $w$ is a diagnostic variable now, $w=\tau+R_a b_1$, obtained from Eq. (12). According to the eigenvalues of the stability matrix, $A$ and $C$ are stable spirals while $B$ is an unstable saddle point.

Box models are widely used to mimic the multiple states of the ocean.[1–3] In these papers, a frictional balance was used to determine the meridional transport, based on the idea that the adjustment time scale of the temperature and salinity fields is much longer than that of the velocity fields. The resulting steady states correspond to having an infinitely

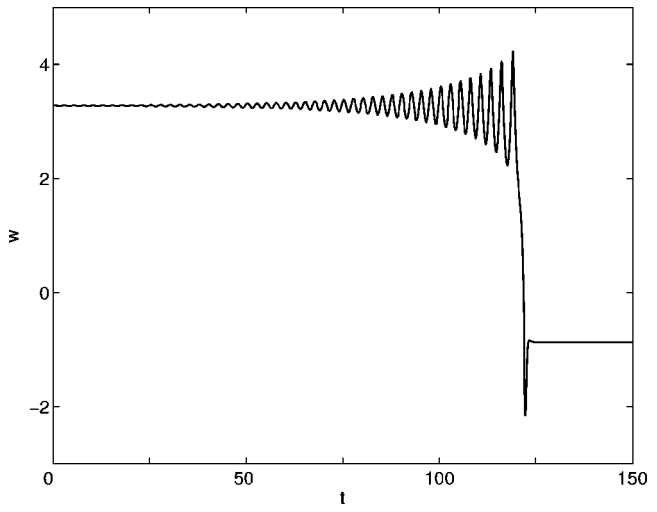


FIG. 11. Time evolution of $w(t)$ with initial conditions $w=3.277$, $a_1=-0.395$, $b_1=-0.120$. The parameters are $P_r=20$, $\tau=4$, and $R_a=6$. The given initial conditions are the stable steady solutions corresponding to $P_r=10$.

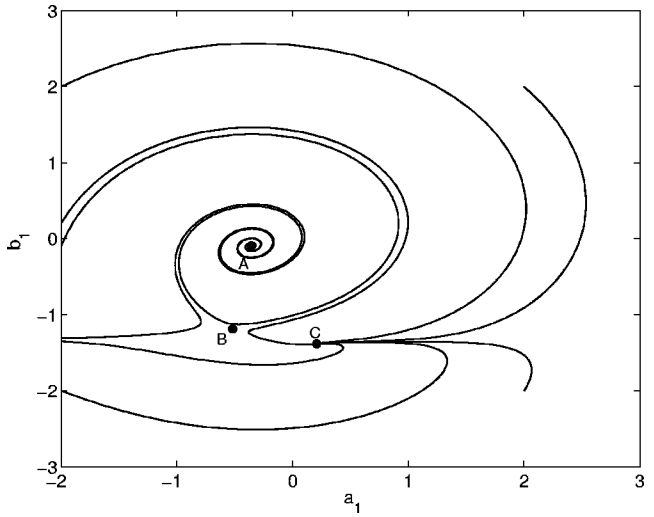


FIG. 12. Time evolution of $a_1$ and $b_1$ with different initial conditions. The parameters are $\tau=4$, $R_a=3$, and $P_r=+\infty$. Points *A* and *C* are stable spirals; *B* is an unstable saddle point.

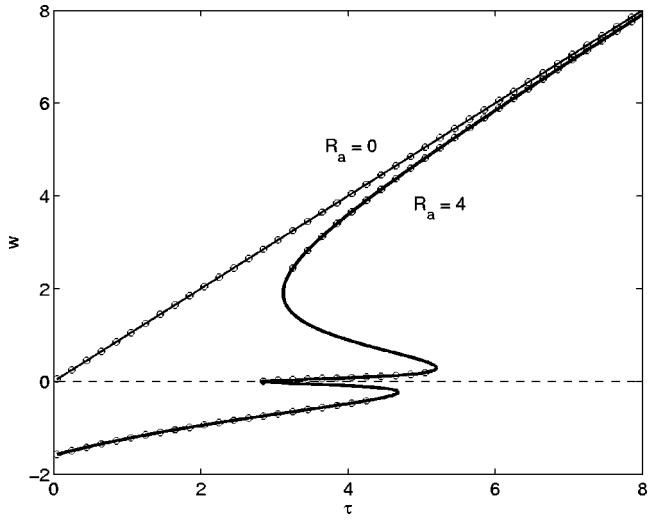


FIG. 13. Roots of Eq. (24) for $w(\tau)$ with $P_r=10$ corresponding to $R_a=0$ (thin line) and $R_a=4$ (thick line). The parameters are $D=0.005$, $\lambda=0.1$, and $P_r=4$.

large Prandtl number in the loop model, as shown in Figs. 10 and 12. In Fig. 12, only *A* is a thermally driven mode.

Even without salinity forcing, an imposed stress can cause very complex behavior in the circulation and temperature distributions. The final states are sensitive to all the parameters, including $P_r, R_a, \tau$, and the initial conditions.

We now turn to the problem with added salinity forcing.

## IV. SALINITY, TEMPERATURE, AND STRESS

Bryan[26] and many others have used mixed boundary conditions in ocean circulation and climate models. This terminology implies the use of the flux condition for salinity and a restoring one for temperature. Restoring to a climatology is used to either mimic a simple atmospheric feedback or to force the system to be more realistic when it drifts under pure thermal flux boundary conditions. For the one-dimensional loop, the introduction of the restoring term produces a virtual energy source,[10] and the physical reality of the resulting solutions is difficult to assess. We will therefore omit the use of restoring in the present system.

As with temperature, a Fourier series is defined for salinity,

$$S(\phi,t)=\sum_{-\infty}^{\infty}\beta_n(t)e^{in\phi}. \tag{22}$$

The evolution equations can be obtained by substituting Eqs. (8) and (22) into Eqs. (5)–(7), with $\alpha_1=a_1+ib_1$ and $\beta_1=c_1+id_1$:

$$\frac{1}{P_r}\frac{dw}{dt}=R_a b_1-R_a\frac{D}{\lambda}d_1-w+\tau, \tag{23a}$$

$$\frac{da_1}{dt}=-a_1+b_1 w, \tag{23b}$$

$$\frac{db_1}{dt}=-b_1-a_1 w-\sqrt{2}, \tag{23c}$$

$$\frac{dc_1}{dt}=-\lambda c_1+d_1 w, \tag{23d}$$

$$\frac{dd_1}{dt}=-\lambda d_1-c_1 w-\sqrt{2}. \tag{23e}$$

Two more parameters, $D$ and $\lambda$ as defined above, now appear. From the above equations, the steady solutions for $w$ is

$$\sqrt{2}R_a\left(-\frac{1}{1+w^2}+\frac{D}{\lambda^2+w^2}\right)=w-\tau. \tag{24}$$

Here we confine ourselves to exploring only a limited parameter range.

### A. Identical thermal/salinity diffusivities

With equal thermal and salinity diffusivities, Eq. (24) reduces to

$$\sqrt{2}R_a(D-1)=(w-\tau)(1+w^2). \tag{25}$$

Clearly, the salinity forcing appears only as a direct counter-effect of the thermal forcing, the extent to which depends on the value of the parameter $D$, a conclusion dependent upon the linear equation of state.

This configuration is interesting only when temperature and salt diffusivities differ (double diffusion), or when restoring is applied to at least one of temperature and salinity (as in S61) thus producing an effective "double diffusion."

### B. Different thermal/salinity diffusivities

Diffusivity is infinite in the S61 model and in most of its successors, so that restoring boundary conditions are necessary there for the presence of multiple states. However, multiple equilibria can also be found because of double-diffusive process. As an example, fix $\lambda=0.1$, $D=0.005$, and $P_r=10$. The steady solutions $w(\tau)$ and their stability properties are displayed in Fig. 13. When $R_a=0$, the system is stress driven

again, but if the Rayleigh number is increased to $R_a=4$, multiple states are found. Now in the parameter range $3.5<\tau<5.9$, five solutions appear, with three stable ones. Compared with Fig. 5, the upper branch in Fig. 13, to some extent, can be regarded as stress dominant; the middle stable branch, salinity dominant; the lower stable branch, thermally dominant. In contrast to box models, this model has one more stress-driven mode. Again, when the circulation is in the stress dominant branch, the circulation rate is only slightly smaller than that without thermal and salinity forcings.

Due to the difference in diffusivities, the introduction of salinity forcing yields one more stable mode. Using the same methods as above, we can find a similar behavior as discussed in last section, but no qualitatively different result is expected.

## V. ENERGY CONSIDERATIONS

Much of the recent literature relevant to the loop-Stommel models concerns the issue of the energy sources driving the ocean circulation.[13–16,27] As already noted, restoring boundary conditions introduce the possibility of unphysical energy sources. More generally,[18] although the ocean circulation involves truly massive energy reservoirs, it is only the comparatively modest inputs of energy from the surface (and the tides of the abyss) that appear to sustain the circulation.

With molecular mixing, as in the experiments of Rossby[28] and Wang and Huang,[16] the internal energy of the fluid is the source of the mixing motions. In the ocean, the turbulence induced mechanically by wind and tides is required. Whether type 3 convection can generate an intense enough large scale flow to produce a turbulent, mixed, interior with finite stratification remains a point of serious contention in the literature.[15,16,27] Even the definition of "turbulence" is in dispute, and as the loop-Stommel model cannot develop three-dimensional motions, this interesting subject is not pursued here.

## VI. CONCLUSIONS

Although initially appearing to be a simple system, the one-dimensional circular loop exhibits remarkably intricate behavior, including the chaotic regime of the Lorenz[21] system. Stress forcing changes the behavior both qualitatively and quantitatively. Given the dominance of the wind field in determining the oceanic circulation, and the use of loop-Stommel models as a circulation analog, an awareness of the influence of stress becomes very important. The stability and evolution of various regimes depends not only upon the thermal and salinity Rayleigh numbers, but also on the Prandtl number, the stress sign and magnitude, and the time history of the introduction of the various forcing functions. Stress effects, here appearing as a body force, in particular, can greatly change the solutions derived from buoyancy forcing alone.

An interesting complication arises from the likelihood that the mixing coefficients, and hence the Rayleigh and Prandtl numbers, are controlled by the magnitude of $\tau$. If an appropriate simple parametrization were known, one could explore the behavior of a system even more directly dependent upon the windstress. Such exploration, without a known parametrization, is beyond our intended scope.

Application of the loop-Stommel models to an analysis of the behavior of three-dimensional global circulation models (GCMs) and to the real ocean must be done very cautiously. The extent to which a three-dimensional circulation resulting from buoyancy and stress forcing can be reduced to the behavior of a one-dimensional loop model remains unclear. If it is a valid reduction, one has achieved a notable simplification of the ocean modeling problem, but demonstrating such validity is again beyond our present scope.

## ACKNOWLEDGMENTS

This work was supported in part by the National Ocean Partnership Program (NASA, NSF). The authors had helpful comments from R. Ferrari, R. X. Huang, and K. Vaage. Helpful comments from the two anonymous referees are also gratefully acknowledged.

## APPENDIX A: STABILITY ANALYSIS

Regular stability analysis is used to determine the stability of the steady solution. We consider small deviations from the steady state, writing $w=\overline{w}+w'$, $a_1=\overline{a_1}+a_1'$, and $b_1=\overline{b_1}+b_1'$, where $\overline{w}$, $\overline{a_1}$, and $\overline{b_1}$ are the corresponding steady solutions, and can be calculated from Eq. (16),

$$\overline{y}-\overline{x}+\tau=0,$$

$$r\overline{x}-\overline{y}-\overline{xz}=0,$$

$$\overline{xy}-\overline{z}=0.$$

It is obvious that they are equal to the values obtained from Eq. (19). At the same time, the linearized equations describing $w'$, $a_1'$, and $b_1'$ are obtained:

$$\frac{dx'}{dt}=\alpha(y'-x'),$$

$$\frac{dy}{dt}=rx'-y'-\overline{x}\overline{z}'-\overline{z}\overline{x}',$$

$$\frac{dz'}{dt}=\overline{x}\overline{y}'+\overline{y}\overline{x}'-z'.$$

Introduce a time factor by letting

$$x'=\hat{x}e^{\sigma t},\quad y'=\hat{y}e^{\sigma t},\quad z'=\hat{z}e^{\sigma t}.$$

Substituting into the equations above, we obtain

$$\begin{pmatrix}-\alpha & \alpha & 0\\ r-\overline{z} & -1 & -\overline{x}\\ \overline{y} & \overline{x} & -1\end{pmatrix}\begin{pmatrix}\hat{x}\\ \hat{y}\\ \hat{z}\end{pmatrix}=\sigma\begin{pmatrix}\hat{x}\\ \hat{y}\\ \hat{z}\end{pmatrix}.$$

Solving the eigenvalue problem of the perturbation matrix determines the stability of the steady solutions to tiny pertur-

bations [see the works of Welander[6] or Strogatz[23] (pp. 129–138) for more examples].

## APPENDIX B: HEAT TRANSPORT IN A STEADY STATE

In a steady state, Eq. (5) can be solved directly in real exponentials,

$$T(\phi) = \begin{cases} C_1 + C_2 e^{w\phi}/w, & -\pi/4 < \phi < \pi/4 \\ C_3 + C_4 e^{w\phi}/w, & \pi/4 < \phi < 7\pi/4, \end{cases}$$

where $C_j$ ( $j=1, 2, 3, 4$) are arbitrary constants. The matching conditions for temperature at $\phi=-\pi/4$ and $\phi=\pi/4$ are

$$(C_2 - C_4)e^{w\pi/4} = w(C_3 - C_1),$$

$$C_2 e^{-w\pi/4} - C_4 e^{7w\pi/4} = w(C_3 - C_1).$$

Integrating Eq. (5) from $\phi=\pi/4-\epsilon$ to $\phi=\pi/4+\epsilon$ yields the flux condition

$$w(C_3 - C_1) = 2\pi.$$

The final mean temperature is the same as that initially ($\oint T d\phi = 0$ in this case), so

$$C_1 + 3C_3 = 0,$$

where the matching conditions have been used. Using the two conditions above, we can calculate the heat transport

$$F(\phi) = \begin{cases} wC_1 = -3\pi/2, & -\pi/4 < \phi < \pi/4 \\ wC_3 = \pi/2, & \pi/4 < \phi < 7\pi/4, \end{cases}$$

whose ratio remains unchanged under different controlling parameters. The distribution of temperature can be obtained by finding $C_1$, $C_2$, $C_3$, and $C_4$.


[1] H. Stommel, "Thermohaline convection with two stable regimes of flow," Tellus **13**, 131 (1961).
[2] C. Rooth, "Hydrology and ocean circulation," Prog. Oceanogr. **11**, 131 (1982).
[3] R. X. Huang, J. Luyten, and H. Stommel, "Multiple equilibrium state in combined thermal and saline circulation," J. Phys. Oceanogr. **22**, 231 (1992).
[4] R. X. Huang and H. Stommel, "Convective flow patterns in an 8-box cube driven by combined wind stress, thermal, and saline forcing," J. Geophys. Res. **97**, 2347 (1992).
[5] J. B. Keller, "Periodic oscillations in a model of thermal convection," J. Fluid Mech. **26**, 599 (1966).
[6] P. Welander, "On the oscillatory instability of a differentially heat fluid loop," J. Fluid Mech. **29**, 17 (1967).
[7] W. V. R. Malkus, "Non-periodic convection at high and low Prandtl number," Mem. Soc. R. Sci. Liege Collect. in-4, 6th Ser. **IV**, 125 (1972).
[8] W. K. Dewar and R. X. Huang, "On the forced flow of salty water in a loop," Phys. Fluids **8**, 954 (1996).
[9] R. X. Huang and W. K. Dewar, "Haline circulation: Bifurcation and chaos," J. Phys. Oceanogr. **26**, 2093 (1996).
[10] C. Wunsch, "Thermohaline loops, Stommel box models, and Sandström's theorem," Tellus, Ser. A **57**, 84 (2005).
[11] C. Wunsch, "Speculations on a schematic theory of the Younger Dryas," J. Mar. Res., **63**, 315 (2005).
[12] H. Stommel and C. Rooth, "On the interaction of gravitational and dynamic forcing in simple circulation models," Deep-Sea Res. **15**, 165 (1968).
[13] W. Munk and C. Wunsch, "Abyssal recipes II: Energetics of tidal and wind mixing," Deep-Sea Res., Part I **45**, 1976 (1998).
[14] R. X. Huang, "Mixing and energetics of the oceanic thermohaline circulation," J. Phys. Oceanogr. **29**, 727 (1999).
[15] F. Paparella and W. R. Young, "Horizontal convection is non-turbulent," J. Fluid Mech. **466**, 205 (2002).
[16] W. Wang and R. X. Huang, "An experimental study on thermal circulation driven by horizontal differential heating," J. Fluid Mech. (in press).
[17] C. Wunsch, "What is the thermohaline circulation?" Science **298**, 1180 (2002).
[18] C. Wunsch and R. Ferrari, "Vertical mixing, energy, and the general circulation of the oceans," Annu. Rev. Fluid Mech. **36**, 281 (2004).
[19] W. Wang and R. X. Huang, "Wind energy input to the Ekman layer," J. Phys. Oceanogr. **34**, 1267 (2004).
[20] J. Pedlosky, *Ocean Circulation Theory* (Springer, Berlin, 1967).
[21] E. N. Lorenz, "Deterministic non-periodic flow," J. Atmos. Sci. **20**, 130 (1963).
[22] D. J. Tritton, *Physical Fluid Dynamics 2nd* (Oxford University Press, Oxford, 1988).
[23] S. H. Strogatz, *Nonlinear Dynamics and Chaos* (Addison-Wesley, Reading, MA, 1994).
[24] T. N. Palmer, "A nonlinear dynamical perspective on climate prediction," J. Clim. **12**, 575 (1999).
[25] A. Adcroft, J. R. Scott, and J. Marotzke, "Impact of geothermal heating on the global ocean circulation," Geophys. Res. Lett. **28**, 1735 (2001).
[26] F. Bryan, "High-latitude salinity effects and interhemispheric thermohaline circulations," Nature (London) **323**, 301 (1986).
[27] J. C. Mullarney, R. W. Griffiths, and G. O. Hughes, "Convection driven by differential heating at a horizontal boundary," J. Fluid Mech. **516**, 181 (2004).
[28] T. Rossby, "On thermal convection driven by non-uniform heating from below: An experimental study," Deep-Sea Res. **12**, 9 (1965).